

## **Effects of Design Parameters on Thermal History and Mechanical Behavior of Additively Manufactured 17-4 PH Stainless Steel**

Rakish Shrestha<sup>1,2</sup>, P. Dastranjy Nezhadfar<sup>1,2</sup>, Mohammad Masoomi<sup>1,2</sup>, Jutima Simsiriwong<sup>3</sup>,  
Nam Phan<sup>4</sup>, Nima Shamsaei<sup>1,2\*</sup>

<sup>1</sup>Department of Mechanical Engineering, Auburn University, Auburn, AL 36849

<sup>2</sup>National Center for Additive Manufacturing Excellence (NCAME),  
Auburn University, Auburn, AL 36849

<sup>3</sup>School of Engineering, University of North Florida, Jacksonville, FL 322224

<sup>4</sup>Structures Division, U.S. Naval Air Systems Command, Patuxent River, MD 20670

\*Corresponding author: shamsaei@auburn.edu

### **Abstract**

In this study, the effects of part size on thermal history and mechanical properties of additively manufactured 17-4 PH stainless steel were investigated under monotonic tensile and strain-controlled fatigue loadings. Two sets of specimens were machined from square rods and oversized specimens, which were fabricated using a laser bed powder fusion (L-PBF) process, to introduce variation in specimen geometry and consequently thermal history. Monotonic tensile tests were conducted at a strain rate of  $0.001 \text{ s}^{-1}$ . Fully-reversed ( $R_e = -1$ ), strain-controlled fatigue tests were performed at 0.003 and 0.0035 mm/mm, and varying test frequency to maintain a constant average strain rate in all tests. Experimental results indicated minimal effect of specimen geometry on the tensile properties of L-PBF 17-4 PH SS, which were also found to be comparable to the wrought material. On the other hand, some influence of specimen geometry on fatigue behavior was observed. Specimens machined from square rods exhibited slightly higher fatigue resistance as compared to specimens machined from oversized specimens. Furthermore, thermal simulations demonstrated higher bulk heating in specimens machined from oversized specimens as compared to those from square rods, which indicated the effect of part geometry on thermal history experienced by the fabricated part.

**Keywords:** Fatigue; Thermal Simulation; Additive manufacturing; Laser-based powder bed fusion (L-PBF)

### **Introduction**

Additive manufacturing (AM) technologies have enabled designers to fabricate application-specific, customized parts with complex geometries. With the capability of producing complete assemblies, AM is also being considered as a cost-effective manufacturing process as it minimizes the number of part assemblies and cost. Due to these advantages, AM has transitioned from a traditional means of rapid prototyping to a tool for advanced manufacturing [1]. There is

also an increased interest in recent years from academia, private industries, and governmental sectors towards AM technologies in effort to fabricate high quality parts with optimal mechanical properties.

Although AM possesses various advantages, the susceptibility of AM parts to inherent defects, such as pores resulting from entrapped gases and voids from lack of fusion (LoF) between the subsequent layers, is one of the major drawbacks of AM processes. As the fatigue resistance of structural parts/components are sensitive to defects, the trustworthiness of AM parts is not fully established, particularly for load bearing and fracture-critical parts in aerospace and automotive applications. Furthermore, it is known that thermal history experienced by AM parts during the manufacturing process is directly affected by the combination of process parameters, such as laser power, hatch spacing, layer thickness, scan speed, etc. Each combination of these parameters can result in variation of parts' thermal history, which, in turn, directly affects their microstructural characteristics, and ultimately mechanical properties of parts [2-4].

In addition, size and geometry of fabricated parts can influence thermal history. Part size can directly dictate the amount of solidified area available for the heat to dissipate through the previously deposited layers. The geometry of the fabricated part can influence the amount of heat dissipating through previously solidified layers and the powder bed, which could result in different thermal histories even within the same layer. Therefore, a combination of different process parameters along with part size and geometry can locally affect cooling rate, temperature gradient, as well as bulk heating during the fabrication. As a result, a thorough study on the effect of part size and orientation is necessary to accurately relate the mechanical behavior of test specimens to a large component with complex geometries, with the end goal of establishing process-structure-property-performance relationship between the test specimens and actual components [5].

Weingarten et al. [6] studied the effects of various process parameters on hydrogen-entrapped pore density in Al-Si-10Mg alloy, which was fabricated using a laser powder bed fusion (L-PBF) process. Among various process parameters including scan speed, hatch spacing, and laser beam diameter, which governs the time between melting and solidification ( $t_M$ ) of melt pool was reported to have the most significant effect on pore density. As  $t_M$  is inversely related to the scan speed, higher scan speed results in lower  $t_M$ . This decreases the time for hydrogen (present as moisture in the powder) to escape from the melt pool, and increases the concentration of hydrogen that transforms into pores during the solidification process.

Similarly, Yang et al. [7] also conducted a study to obtain the effects of process parameters and part geometry on the mechanism of pore formation in L-PBF Al-7Si-Mg and L-PBF Al-10Si-Mg. The volumetric (i.e. energy per unit volume) and areal (i.e. energy per unit area) energy density, which are functions of laser power, scan speed, hatch distance, and layer thickness were related to the formation of different types of defects including, LoF defects, small gas pores, and large keyhole-type pores. Larger LoF defects were attributed to the lower volumetric energy density resulting from higher scan speed. On the other hand, formation of small gas pores were seen to be affected from moisture present in the powder and high areal energy density. Large round pores were reported to be associated with the keyhole mode of melting due to high volumetric energy density. Furthermore, the effect of part geometry on the distribution of defects was investigated by fabricating a special type of specimen that consists of cubic geometry at the bottom, cylindrical in the middle section, and thin plate at the top. It was found that the thin plate section contained higher amount of porosity level as compared to the other two sections. This was

attributed to the smaller cross-section area available for heat dissipation as well as use of meander scan speed [7]. Hengfeng et al. [8] investigated the effect of energy density as a function of laser power, hatch spacing, and layer thickness on the porosity of AM PH 17-4 SS. It was found that, at high scan speed and laser power, pores were formed due to balling phenomenon and thermal stress cracking, while low laser power and scan speed produced LoF crevices due to insufficient melting [8].

Recently, Pegues et al. [9] studied the effect of specimen surface area and gage section radius on fatigue behavior of diagonally-built AM Ti6Al4V alloy in as-built condition. Results showed that the gage section radius had more effect on fatigue resistance as compared to the surface area. Furthermore, as specimens were fabricated at 45° with respect to the substrate, the majority of heat is dissipated from the previously solidified layer in the top-skin surface (surface facing away from the substrate), while for the down-skin (surface facing towards the substrate) surface, heat is mostly dissipated through powder. As the heat transfer coefficient for solidified part is higher than the powder, there is a distinction of the thermal history between the top- and down-skin surfaces, leading to difference in surface roughness. Additionally, fracture surfaces also revealed that cracks always initiated from the down-skin surface that had higher surface roughness, indicating a significant effect of part geometry on the corresponding thermal history variation, and consequently fatigue behavior.

To better understand the fatigue behavior in AM materials, the formation of defects resulting from thermal history experienced by the fabricated parts should be investigated. In this study, the effects of part geometry on monotonic tensile and fatigue behavior of L-PBF 17-4 precipitation hardening (PH) stainless steel (SS) are investigated in attempt to relate the variation and distribution of defects. The material in this study, 17-4 PH SS, is currently of interest in various applications due to its corrosion resistance coupled with high yield and ultimate tensile strengths. These include aerospace (particularly in turbine blade designs), marine, nuclear power plants, as well as in oil and gas industries. Following the introduction in this study, the material and experimental procedures are presented. The experimental results are then discussed along with the fractography analysis and thermal simulations. Finally, important conclusions are drawn.

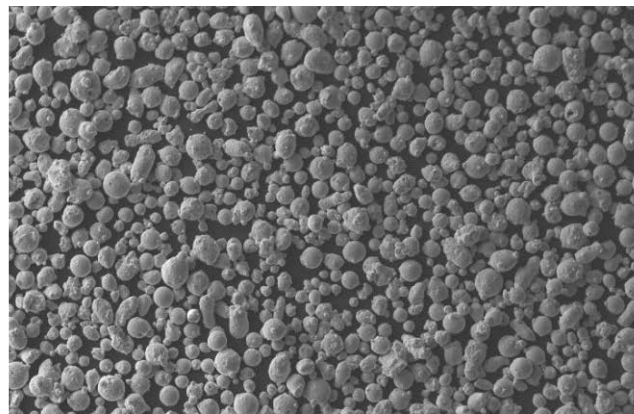
### **Material and Experimental Procedures**

Argon atomized 17-4 PH SS powder produced by LPW Inc. with size distribution ranging from 15-45 µm was used to fabricate specimens using an EOS M290, a L-PBF system. The employed process parameters are shown in Table 1. Furthermore, shape distribution of the utilized powder was also investigated using a scanning electron microscope (SEM) and shown in Fig. 1(a). SEM image revealed that the majority of the powder particle were spherical in shape with average size of 25 µm.

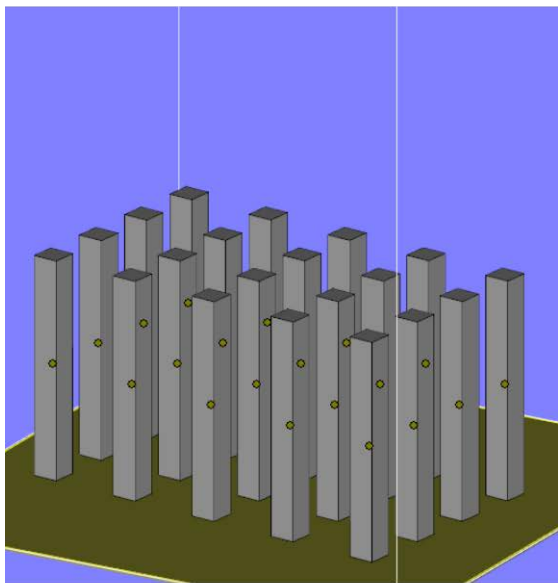
**Table 1:** Process parameter used to fabricate the L-PBF PH 17-4 SS specimens

<b>Laser power (W)</b>	<b>Scanning speed (mm/s)</b>	<b>Hatching distance (µm)</b>	<b>Layer thickness (µm)</b>
<b>220</b>	755.5	100	40

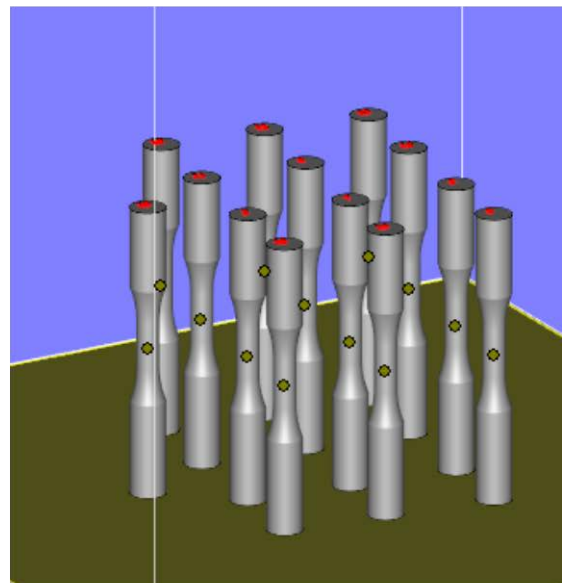
The two sets of specimens, one from vertically-built L-PBF PH 17-4 SS square rods with dimensions 12x12x90 mm shown in Fig. 1(b) and another set of vertically-built L-PBF PH 17-4 SS oversized specimens with gage diameter of 8 mm in Fig. 1(c), were machined using a CNC lathe. The specimen dimensions with uniform gage section, following ASTM E606 [10] standard, are presented in Fig. 2. For simplicity, the specimens fabricated from square rods and oversized specimens will be referred to as Specimen Set A and Specimen Set B, respectively, throughout this manuscript. All specimens were subjected to CA H 1025 heat treatment, which was selected based on a study of effects of different heat treatment on the mechanical behavior of 17-4 PH SS, which is currently under preparation. To eliminate the effect of surface roughness, specimens were further polished using different grit sandpapers to remove all the horizontal machining marks.



(a)



(b)



(c)

**Figure 1:** (a) SEM image of PH 17-4 SS powder along with L-PBF PH 17-4 SS parts built in vertical direction with two different specimen geometries including (b) 12x12x90 mm square rod and (c) oversized specimen with gage diameter of 8 mm.

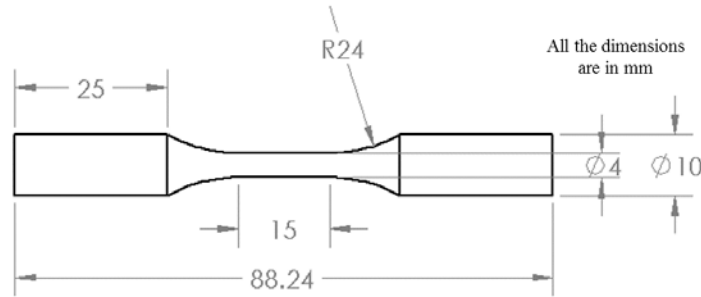


**Figure 2:** Specimen geometry for monotonic tensile and fatigue tests fabricated based on ASTM E606 standard [10].

The mechanical testing, including monotonic tensile and fatigue tests, were performed using a servo hydraulic MTS landmark test frame with the load capacity of 100 kN. All tests were conducted in strain-controlled mode, and the axial strain was measured and controlled using a mechanical extensometer with 10 mm gage length. As elongation to failure of 17-4 PH SS exceeded the allowable travel distance of the extensometer, monotonic tensile tests were first conducted at strain rate of  $0.001 \text{ s}^{-1}$  under strain-controlled mode, and later switched to displacement-controlled mode. Fully-reversed ( $R_\varepsilon = -1$ ) uniaxial strain-controlled fatigue tests were carried out at 0.003 and 0.0035 mm/mm strain amplitudes. The test frequencies were varied to maintain similar strain rate in all fatigue tests to eliminate any strain rate effect.

### **Physical Model and Numerical Method**

A major challenge in simulating the AM process is to develop an efficient model that can produce information and knowledge at the overall scale of the desired part and build-process to inform engineering decisions [11, 12]. There can be kilometers of laser travel length and thousands of powder layers in a single build, thus presenting a computational challenge. To be useful, part-scale simulations must be executable in a reasonable amount of time, while still retaining sufficient physical fidelity to yield trustworthy results. An eventual goal is to have efficient process models that could be included as a part of an automated process optimization.

At the part scale, one neglects the details of local laser-powder interaction. Instead, the goal is to describe part thermomechanical behavior both during and after the build is completed. In this approximation, the powder was represented as a reduced-density, low-strength solid. The deposition of the laser energy into the powder was then represented by a volumetric energy source term such as that derived by Gusarov et al. [13]. Melting was represented thermally through a latent heat parameter and mechanically as a near-total loss of strength. The “mushy zone” at the

melt pool boundary was represented by having its temperature-dependent strength rise as temperature falls below the solidus temperature.

For modeling, each layer is typically simulated separately with the per-island scan strategy. In the proposed numerical method, the heat flux at the top layer was assumed to be uniform. The total amount of time that the heat flux is applied was based on the time required to build one layer. In the case of rectangular section shown in Fig. 3(a), the time period was calculated as:

$$t = \frac{m \times l}{w \times v} \quad (1)$$

where  $l$  is the length of the rectangle,  $m$  is the thickness of the part,  $w$  is the hatching space, and  $v$  is scanning speed. Similarly, the total time to fabricate a slice of a cylindrical part with circular cross-section of diameter of  $D$  as shown in Fig. 3(b), is calculated as:

$$t = \frac{m \times l \pi D^2 / 4}{w \times v m \times l} = \frac{\pi D^2 / 4}{w \times v} \quad (2)$$

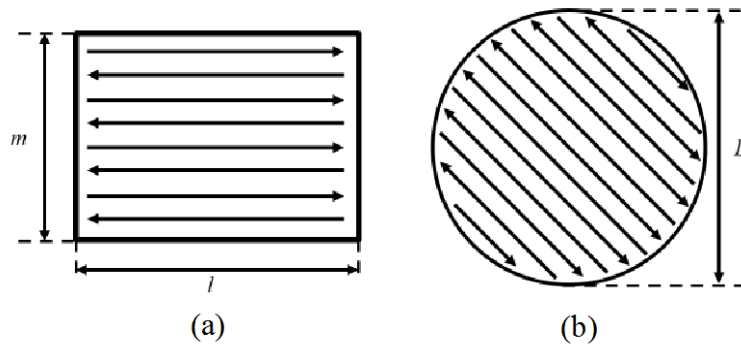


**Figure 3.** Schematic of built area for (a) the square rod and (b) the oversized specimen.

The constant heat flux applied at the top of the layer,  $q_{pb,i}$ , is calculated as:

$$q_{pb} = \frac{P}{m \times l} \quad (3)$$

$$q_{pb} = \frac{P}{\pi D^2 / 4} \quad (4)$$

where  $P$  is laser power. Another assumption used to facilitate the simulation was to attach layers together to form a bulk-layer, which significantly decreased the number of layers required to model the AM part.

## Experimental Results and Discussions

Engineering stress-strain responses obtained from the monotonic tensile tests for two sets of L-PBF PH 17-4 SS specimens are displayed in Fig. 4. As explained in the previous section, the stress-strain responses were captured up to the extensometer's limit prior to switching from strain- to displacement-controlled mode. The corresponding tensile properties are shown in Table 2 and compared to those of wrought material reported in [14]. As seen in Fig. 4, the effect of specimen geometry on the tensile behavior is not significant. Tensile properties for L-PBF PH 17-4 SS specimens were comparable to the wrought material (10% difference in yield strength and 16% difference in ultimate tensile strength).

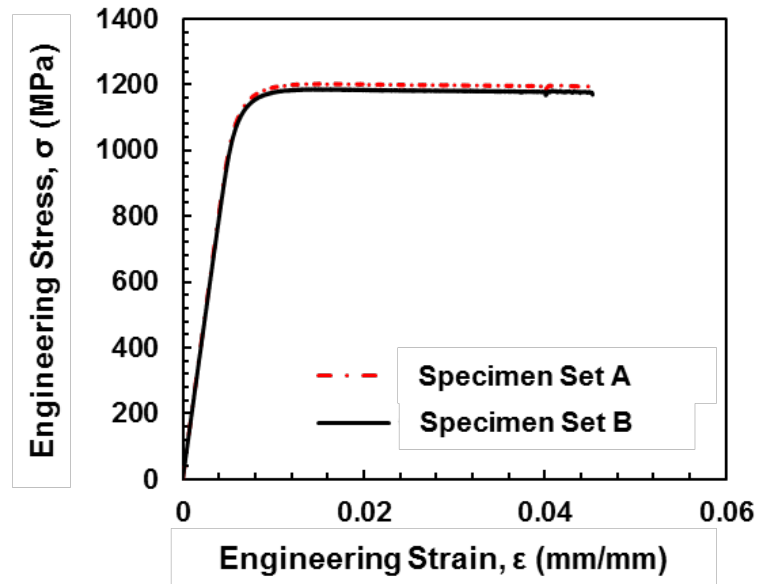


**Figure 4:** Engineering stress-strain responses for L-PBF PH 17-4 SS specimens.

**Table 2:** Tensile properties of L-PBF and wrought PH 17-4 SS specimens.

Specimen Geometry	$\sigma_y$ (MPa)	$\sigma_u$ (MPa)	E (GPa)
L-PBF Specimen Set A	1170	1203	205
L-PBF Specimen Set B	1160	1188	202
Wrought [14]	1070	1000	200

To obtain the failure mechanism and defect distribution in specimens, fractography analysis was conducted on the failed tensile specimens. Fracture surface for Specimen Set A and Specimen Set B are shown in Figs. 5(a) and 5(b), respectively. Both types of specimen geometry

exhibited a cup and cone type fracture surface as well as dimples, indicating a ductile failure. Moreover, these dimples can also show the presence of precipitates common in PH SS. The Cu-rich precipitates become coarser and non-coherent to the matrix due to high temperature heat treatment for longer period of time (i.e. CA-H1025). As a result, dislocations must bypass these coarse non-coherent precipitates, which can lead to difference in the deformation rate of matrix and precipitates and consequently formation of dimples [15]. Additionally, some facets representing brittle fracture behavior as pointed out by the white arrows in Fig. 5 were also seen on the fracture surfaces. These observations may suggest that the failure mode of L-PBF 17-4 PH SS under monotonic tensile loading may be a combination of both ductile and brittle fracture. Furthermore, some secondary cracks, denoted by the red solid arrows in Fig. 5(a), were observed only in Specimen Set A, while they were absent in Specimen Set B. However, these cracks seem to have minimum effect, as the tensile properties as both sets of specimen were similar, as seen in Fig. 4, and comparable to the wrought counterpart.

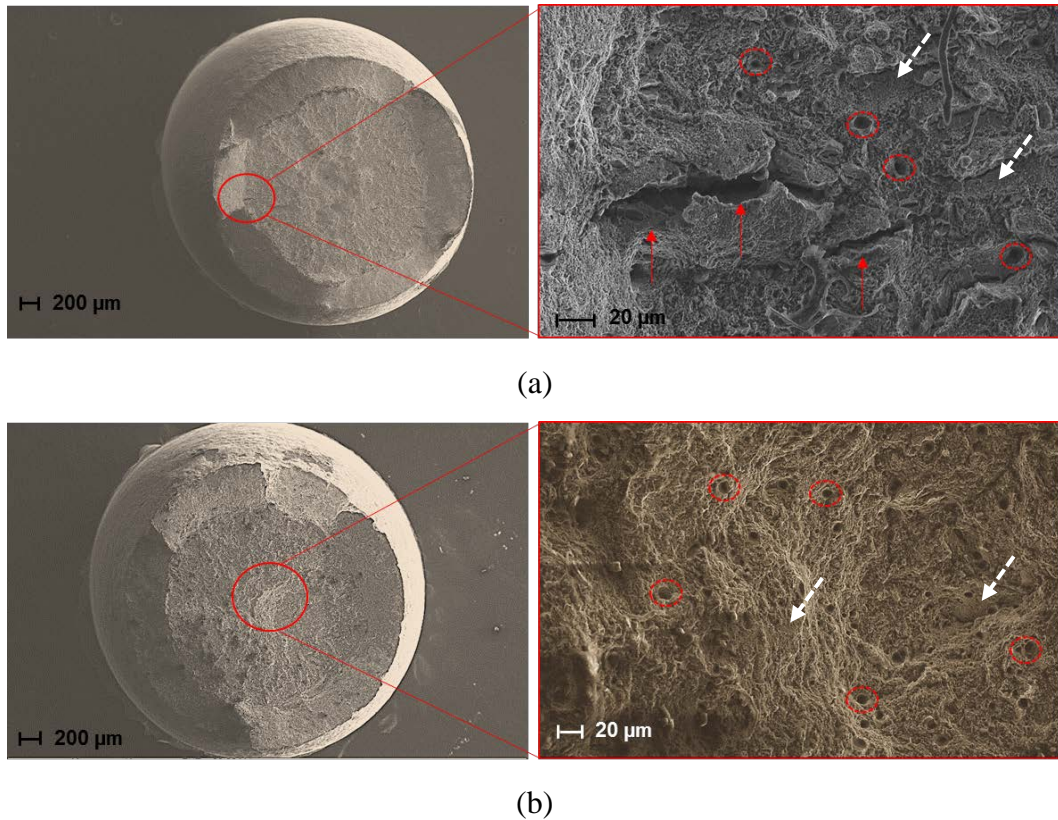


**Figure 5:** Fracture surfaces for specimens fabricated from (a) Specimen Set A and (b) Specimen Set B failed under monotonic tensile loading.

Although the presence of defects may not have a substantial impact on the monotonic tensile properties, defects can significantly affect the fatigue behavior of AM materials, which is more defect-driven. Such observation was also noted in the previous study on L-PBF 316L SS [16]. Fatigue lives for two sets of specimens under uniaxial, fully-reversed strain-controlled

condition are displayed in Fig 6. As seen, Specimen Set A exhibited better fatigue resistance when compared to Specimen Set B, approximately by a factor of 3 and 1.5 in lower (0.003 mm/mm) and higher (0.0035 mm/mm) strain amplitude tests, respectively. More scatter in fatigue data at lower strain amplitude is also evident in this figure. Such result can be attributed to the fact that, at lower strain amplitudes the failure mechanism is more defect driven compared to the high strain amplitude loading [17]. Therefore, fatigue lives at lower strain amplitude are more sensitive to location, size, and types of defects, which can add scatter in the fatigue data. Nonetheless, a distinct variation in the fatigue lives between Specimen Set A and Set B can be observed in Fig 6, suggesting the effect of part geometry on fatigue life of L-PBF 17-4 PH SS specimens.

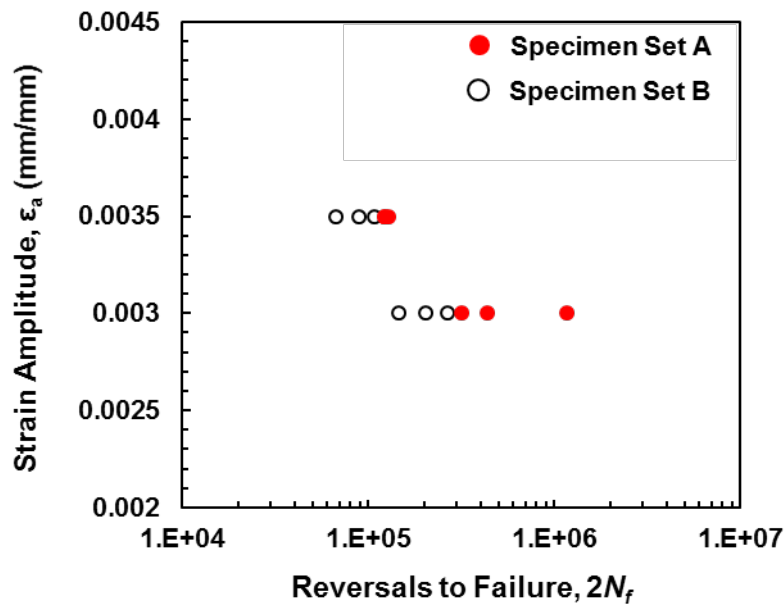
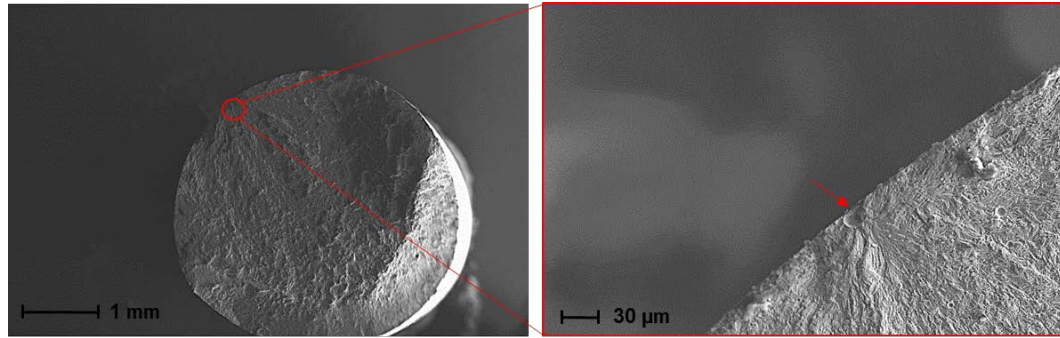
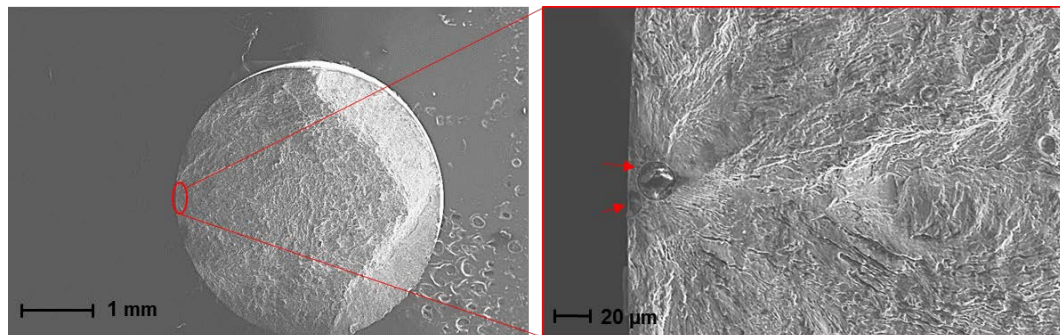


**Figure 6:** Strain-life data showing variation in fatigue life of 17-4 PH SS specimens.

Figures 7(a) and 7(b) display the fracture surface of Specimen Set A (317,060 reversals) and Specimen Set B (145,330 reversals), respectively, both subjected to strain amplitude of 0.003 mm/mm. As can be seen, the fatigue crack in Specimen Set B initiated from two gas pores at the specimen's surface. On the other hand, for the Specimen Set A, crack was observed to initiate from a single pore, also at the surface of the specimen. Similar observation with the crack initiating from multiple pores was also seen in another specimen from Specimen Set B, which may have resulted in lower fatigue resistance as compared to Specimen Set A. It is to be noted that X-ray computed tomography should be conducted to determine the distribution of defects in each set of specimens, followed by further fractography analysis to accurately conclude the results.



(a)



(b)

**Figure 7:** Fracture surfaces showing crack initiating factors for specimens fabricated from (a) oversized specimen (Specimen Set A) and (b) square rod (Specimen Set B) subjected to 0.003 mm/mm strain amplitude.

### Thermal Simulation and Discussions

As mentioned previously, the variation in thermal history experienced by the fabricated parts can affect the distribution of defects. Therefore, using a thermal simulation tool, the temperature distribution and heat accumulation for two types of specimen geometries was also investigated in this study. Temperature distribution after fabrication of oversized specimens (i.e. Fig 1(c)) and square rods (i.e. Fig. 1(b)), are presented in Fig. 8. It is observed that the temperature at newly deposited layers are higher compared to previously deposited layers. Additionally, higher accumulated heat was seen in the case of the oversized specimen compared to the square rod.

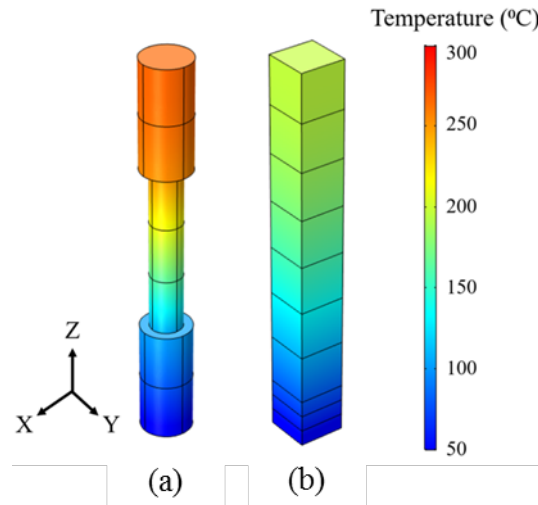


**Figure 8.** Temperature distribution of fabricated (a) oversized specimen and (b) square rod after fabrication of the parts.

Distribution of predicted temperature at different heights of the fabricated parts is shown in Figs. 9(a) and 9(b), respectively, for oversized specimen (i.e. Fig. 1(c)) and square rod (i.e. Fig. 1(b)). As can be seen, after the fabrication, the maximum temperature for oversized specimen was almost  $100^{\circ}\text{C}$  higher compared to the square rod. Such a variation in bulk temperature of the fabricated part can affect the temperature gradient and cooling rate, which can have a significant effect on microstructural features and defect distribution. Hence, variation in the thermal history observed in Fig. 8 may be responsible for differences in fatigue lives exhibited by Specimen Set A and Set B in Fig. 6.

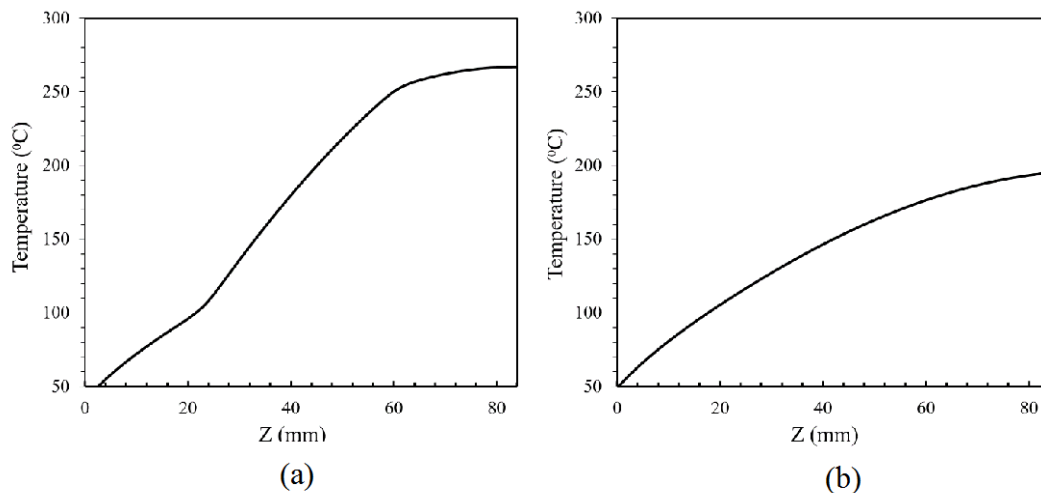


**Figure 9.** Temperature distribution of (a) oversized specimen and (b) square rod along the main axis after fabrication of last layer.

## **Conclusions**

In this study, effects of part geometry on the tensile and fatigue properties of L-PBF 17-4 PH SS were investigated for specimens machined from parts with different sizes. Based on the experimental results and simulations, the following conclusions were drawn:

1. L-PBF 17-4 PH SS specimens machined from square rods and oversized specimens exhibited similar tensile properties, which were also comparable to those reported for the wrought material.
2. Specimens machined from square rods generally possessed better fatigue resistance when compared to the specimens machined from oversized specimens.
3. Thermal simulation results indicated difference in heat accumulation between the oversized specimens and square rods. At the end of the fabrication, the oversized specimens were shown to be approximately 100 °C higher in bulk temperature compared to the square rods. Such variation in thermal history can have significant effects on microstructure, defect distribution, and ultimately fatigue life of the L-PBF 17-4 PH SS.

Results from the current study show that the fractography analysis and thermal simulation alone cannot completely explain the effect of part geometry on the fatigue resistance of L-PBF 17-4 PH SS. Therefore, the relationship between part geometry and thermal history should be further analyzed using microstructural studies to determine the difference in grain structure, and x-ray CT scans to determine the distribution of defects resulting from variations in thermal history.

## **Acknowledgement**

This material is based upon work supported by the Naval Air Systems Command (NAVAIR).

## **References**

- [1] E.C. Santos, M. Shiomi, K. Osakada, T. Laoui, Rapid manufacturing of metal components by laser forming, *International Journal of Machine Tools and Manufacture*, 46, 2006 1459-68.
- [2] A. Yadollahi and N. Shamsaei, Additive manufacturing of fatigue resistant materials: challenges and opportunities, *International Journal of Fatigue*, 98, 2017 14-31.
- [3] S. M. Thompson, L. Bian, N. Shamsaei, and A. Yadollahi, An overview of Direct Laser Deposition for additive manufacturing; Part I: Transport phenomena, modeling and diagnostics, *Additive Manufacturing*, 8, 2015 36-62.
- [4] N. Shamsaei, A. Yadollahi, L. Bian, and S. M. Thompson, An overview of Direct Laser Deposition for additive manufacturing; Part II: Mechanical behavior, process parameter optimization and control, *Additive Manufacturing*, 8, 2015 12-35.
- [5] S. R. Daniewicz and N. Shamsaei, An introduction to the fatigue and fracture behavior of additive manufactured parts, *International Journal of Fatigue*, 94, 2017 1.
- [6] C. Weingarten, D. Buchbinder, N. Pirch, W. Meiners, K. Wissenbach, R. Poprawe, Formation and reduction of hydrogen porosity during selective laser melting of AlSi10Mg, *Journal of Materials Processing Technology*, 221, 2015 112-120.

- [7] K.V. Yang, P. Rometsch, T. Jarvis, J. Rao, S. Cao, C. Davies, X. Wu, Porosity formation mechanisms and fatigue response in Al-Si-Mg alloys made by selective laser melting, *Materials Science and Engineering: A*, 712, 2018 166-74.
- [8] H. Gu, H. Gong, D. Pal, K. Rafi, T. Starr, B. Stucker, Influences of energy density on porosity and microstructure of selective laser melted 17-4PH stainless steel, 2013 Solid Freeform Fabrication Symposium, 2013 474-89.
- [9] J. Pegues, M. Roach, R.S. Williamson, N. Shamsaei, Surface roughness effects on the fatigue strength of additively manufactured Ti-6Al-4V, *International Journal of Fatigue*, Accepted 2018.
- [10] ASTM E606-04, Standard Practice for Strain-Controlled Fatigue Testing, ASTM International, West Conshohocken, PA, 2004.
- [11] R. Martukanitz, P. Michaleris, T. Palmer, T. DebRoy, Z.-K. Liu, R. Otis, T.W. Heo, L.-Q. Chen, toward an integrated computational system for describing the additive manufacturing process for metallic materials, *Additive Manufacturing*, 1-4, 2014 52-63.
- [12] T.M. Rodgers, J.D. Madison, V. Tikare, M.C. Maguire, Predicting Mesoscale Microstructural Evolution in Electron Beam Welding, *JOM*, 68, 2016 1419-26.
- [13] A.V. Gusarov, I. Yadroitsev, P. Bertrand, I. Smurov, Model of Radiation and Heat Transfer in Laser-Powder Interaction Zone at Selective Laser Melting, *Journal of Heat Transfer*, 131, 2009 072101-10.
- [14] ASTM A693-16, Standard Specification for Precipitation-Hardening Stainless and Heat-Resisting Steel Plate, Sheet, and Strip, ASTM International, West Conshohocken, PA, 2016.
- [15] K.-C. Hsu, C.-K. Lin, High-temperature fatigue crack growth behavior of 17-4 PH stainless steels, *Metallurgical and Materials Transactions A*, 35, 2004 3018-24.
- [16] R. Shrestha, J. Simsiriwong, N. Shamsaei, S. M. Thompson, and L. Bian, "Effect of build orientation on the fatigue behavior of stainless steel 316L manufactured via a laser-powder bed fusion process, Solid Freeform Fabrication Symposium-An Additive Manufacturing Conference, Austin, 2016.
- [17] R.I. Stephens, A. Fatemi, R.R. Stephens, H.O. Fuchs, *Metal fatigue in engineering*, John Wiley & Sons 2000.